pyr RNA binding to the *Bacillus caldolyticus* PyrR attenuation protein – characterization and regulation by uridine and guanosine nucleotides

Casper M. Jørgensen[1],*, Christopher J. Fields[1], Preethi Chander[2], Desmond Watt[1], John W. Burgner II[2,3], Janet L. Smith[2,4] and Robert L. Switzer[1]

1 Department of Biochemistry, University of Illinois, Urbana, USA
2 Department of Biological Sciences, Purdue University, Lafayette, IN, USA
3 Bindley Bioscience Center, Purdue University, West Lafayette, IN, USA
4 Life Sciences Institute and Department of Biological Chemistry, University of Michigan, Ann Arbor, USA

The PyrR protein regulates expression of pyrimidine biosynthetic (*pyr*) genes in many bacteria. PyrR binds to specific sites in the 5′ leader RNA of target operons and favors attenuation of transcription. Filter binding and gel mobility assays were used to characterize the binding of PyrR from *Bacillus caldolyticus* to RNA sequences (binding loops) from the three attenuation regions of the *B. caldolyticus pyr* operon. Binding of PyrR to the three binding loops and modulation of RNA binding by nucleotides was similar for all three RNAs. The apparent dissociation constants at 0 °C were in the range 0.13–0.87 nM in the absence of effectors; dissociation constants were decreased by three- to 12-fold by uridine nucleotides and increased by 40- to 200-fold by guanosine nucleotides. The binding data suggest that *pyr* operon expression is regulated by the ratio of intracellular uridine nucleotides to guanosine nucleotides; the effects of nucleoside addition to the growth medium on aspartate transcarbamylase (*pyrB*) levels in *B. subtilis* cells *in vivo* supported this conclusion. Analytical ultracentrifugation established that RNA binds to dimeric PyrR, even though the tetrameric form of unbound PyrR predominates in solution at the concentrations studied.

The PyrR protein regulates expression of the genes of *de novo* pyrimidine nucleotide biosynthesis (*pyr* genes) in nearly all Gram-positive and many other bacteria by a transcription attenuation mechanism [1]. PyrR acts by binding to a segment of *pyr* mRNA with conserved sequence and secondary structure [1,2]. When PyrR is bound, a downstream antiterminator stem-loop structure is prevented from forming, and formation of a transcription terminator is permitted. The affinity of PyrR for *pyr* mRNA is increased by uridine nucleotides [2,3], so an elevated pyrimidine level in the cells results in greater termination of transcription at

sites upstream of the ORF of the *pyr* genes. Three sites of PyrR binding and transcription attenuation have been identified in the *pyr* operons of *Bacillus subtilis* and related *Bacillus* species [1]. These are located in the 5′ untranslated leader of the operon (binding loop 1 or BL1), between the first cistron of the operon, *pyrR*, and the second cistron *pyrP* (BL2), and between *pyrP* and the third cistron *pyrB* (BL3) (Fig. 1A).

All of the initial genetic [4–7] and biochemical [2,3,8,9] studies of the regulation of *pyr* genes by PyrR in our laboratory were conducted with *B. subtilis* strains and PyrR purified from *B. subtilis*. However,

Abbreviation
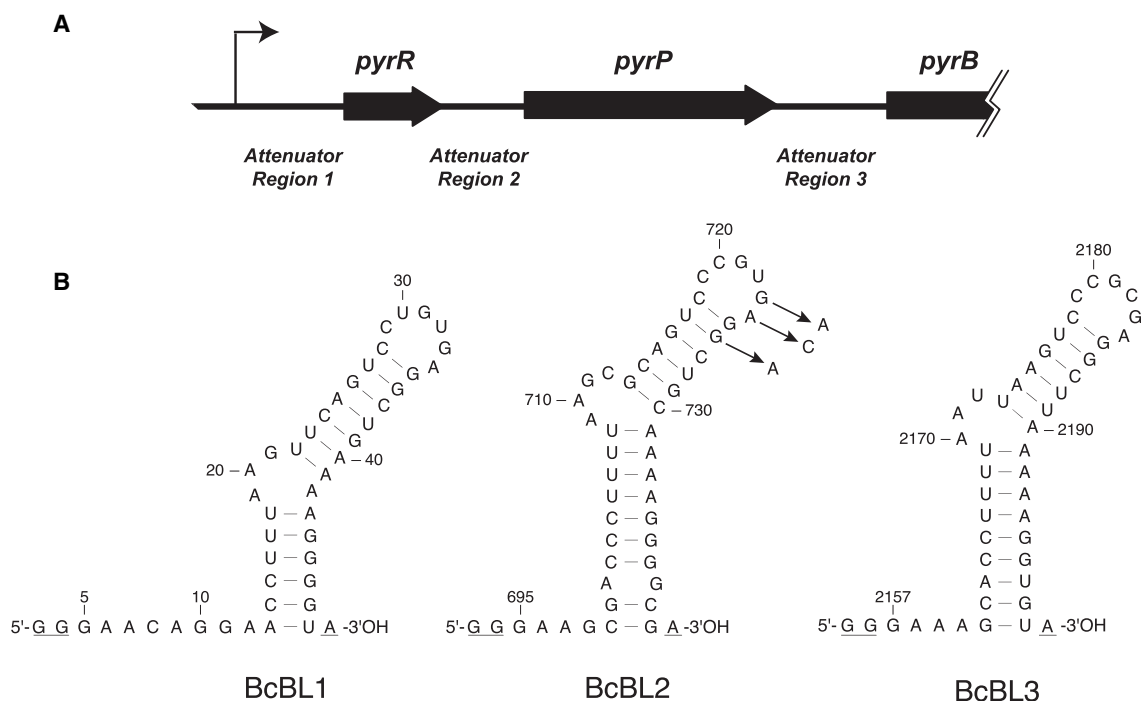
ATCase, aspartate transcarbamylase.

Fig. 1. (A) Map of the 5′-end of the *B. caldolyticus pyr* operon. The thin bent arrow represents the transcriptional start site; ORFs are represented as thick arrows; the untranslated regions containing the three attenuator regions are shown as lines of medium thickness. (B) Sequence of the three *pyr* mRNA species (binding loops) bound by PyrR that were examined. The BcBL1, BcBL2 and BcBL3 sequences were derived from portions of the DNA sequence of attenuator regions 1, 2 and 3, respectively, shown in (A). Numbers refer to the nucleotide number in the *B. caldolyticus pyr* transcript with +1 as the transcriptional start site [13]. The secondary structures were predicted by MFOLD version 3.1 (http://www.bioinfo.rpi.edu/applications/mfold) [32]. Three nucleotides in each binding loop that are not part of the wild-type *pyr* mRNA sequence are underlined: The two first G residues in each transcript are specified by the T7 promoter and the terminal A residue is added by Taq polymerase when used for preparation of templates for *in vitro* transcription by T7 polymerase. Arrows indicate three single-base substitution RNA variants in BcBL2 examined.

PyrR from the closely related thermophilic organism, *Bacillus caldolyticus*, offers advantages for biochemical studies. *Bacillus caldolyticus* PyrR is more stable than the *B. subtilis* homologue. At the concentrations examined, *B. caldolyticus* PyrR exists in solution as a single aggregation state (i.e. the tetramer) and forms crystals that are highly suitable for X-ray crystallographic analysis [10,11]. *Bacillus caldolyticus* offers an excellent alternative system for studies of PyrR-dependent regulation of the *pyr* operon. The organization and regulation of the *B. caldolyticus pyr* operon is essentially the same as in *B. subtilis* [12,13]. Plasmid-borne *B. caldolyticus pyrR* restores normal regulation by pyrimidines to a *B. subtilis* strain in which the *pyrR* gene was deleted [13]. The structures of PyrR proteins from both species have been determined at high resolution [8,10] and the subunit and dimeric structures of the two homologues are essentially identical, although *B. subtilis* PyrR crystallizes as a hexamer or as a dimer, whereas *B. caldolyticus* PyrR is a tetramer [10]. The recent determination of the structure of *B. caldolyticus* PyrR with bound nucleotides led to the unexpected finding that both UMP and GMP bind to equivalent sites on the PyrR dimer [10]. The nucleotide binding sites do not overlap with the likely RNA binding site on PyrR. A preliminary RNA binding study demonstrated that guanosine nucleotides have effects on RNA binding by PyrR that are opposite to the effects of uridine nucleotides [10]. That is, GMP and GTP decrease the affinity of PyrR for *pyr* RNA, whereas UMP and UTP increase its affinity for RNA.

In the present study, we conducted a detailed investigation of the binding of *B. caldolyticus* PyrR to the three RNA sequences to which it binds in *B. caldolyticus*, which we called BcBL1, BcBL2 and BcBL3, and the effects of nucleotides on RNA binding. A rapid and convenient filter binding assay [14] was used for many of these experiments. Electrophoretic mobility shift assays and sedimentation velocity experiments were also used to characterize binding of PyrR to

RNA. Use of the filter binding assay was frustrated in previous studies with *B. subtilis* PyrR because that protein tended to aggregate and failed to bind quantitatively to various hydrophobic filters. However, the filter binding method can be used to study RNA binding to PyrR from *B. caldolyticus*, possibly because this protein has a lower overall negative electrostatic surface potential than the *B. subtilis* homologue [10] and does not aggregate. The present study leads to a more refined characterization of the PyrR–RNA interaction, a definition of binding stoichiometry as one RNA binding loop per PyrR dimer and a definition of the specificity of nucleotide effects on RNA binding. The implications of the the current findings for the physiological regulation of pyrimidine biosynthesis are presented; the most important of these is that regulation of *pyr* operon expression by PyrR relies on shifts in the ratio of uridine nucleotides to guanosine nucleotides, and not the intracellular concentration of uridine nucleotides alone.

Results

Uridine and guanosine nucleotides modulate PyrR binding to all three *pyr* mRNA binding loops

The predicted secondary structures of the three *B. caldolyticus pyr* mRNA binding loops (BcBL1, BcBL2 and BcBL3) examined in the present study are shown in Fig. 1B. All three binding loops contain segments that are conserved in PyrR binding loops from homologous regulatory systems in other bacteria [2]. Conserved features include the predicted stem-loop structure with a purine-rich internal bulge, a terminal hexaloop containing the CNGNGA consensus sequence, and the UUUAA consensus sequence in the lower stem and internal bulge. Filter binding was used to estimate the affinity of the *B. caldolyticus* PyrR protein to each of the three binding loops (Fig. 2A–C). Binding was specific for *pyr* RNA, as shown by the failure of a control RNA (i.e. the antisense strand to BcBL1) to bind to any concentration of PyrR tested (Fig. 2A).

Binding of PyrR to BcBL2 and BcBL3 in standard binding buffer in the absence of effectors followed a binding curve (sigmoid on a semi-log plot of PyrR concentration versus % of total RNA bound) that was indicative of a simple PyrR–RNA binding isotherm (Fig. 2B,C). However, the binding curve for BcBL1 deviated consistently from the fitted curve (Fig. 2A). On the other hand, in the presence of 0.5 mM UMP, which stimulated binding for all three binding loops,

PyrR binding to BcBL1 resembled the binding observed for the other two binding loops. The apparent dissociation constant (K_d) values for RNA binding are shown in Table 1. When no nucleotides were present, PyrR bound most tightly to BcBL2 and BcBL3 (K_d of 0.13 ± 0.02 nM and 0.2 ± 0.08 nM, respectively). The K_d value for PyrR binding to BcBL1 (0.9 ± 0.3 nM) corresponds to slightly looser binding. Addition of 0.5 mM UMP, UDP or UTP resulted in tighter binding, yielding K_d values in the range 0.04–0.09 nM for the three RNAs. PRPP and dUMP also stimulated binding, although not as effectively as UMP.

The apparent K_d values for binding of *B. caldolyticus pyr* binding loops BcBL1, BcBL2 and BcBL3 to PyrR were increased in the presence of GMP by 90-, 40- and 200-fold, respectively, relative to their values in the absence of effector, indicative of a reduced affinity for RNA (Table 1). However, these constants were difficult to determine precisely because the binding data were not adequately fitted by a simple binding equation (Fig. 2A–C). GDP, GTP and dGMP also inhibited binding, although they were less effective at saturating concentrations than GMP (Table 1).

Because all three binding loops bound with similar affinity to PyrR and the effects of nucleotides on RNA binding were similar for all three RNAs, we conducted most of the subsequent studies with a single RNA (BcBL2) because the binding of the homologous *B. subtilis* RNA (BsBL2) was thoroughly investigated in a previous study [2].

Concentrations of nucleotides required for activation or inhibition of PyrR binding to *pyr* binding loops

The concentrations of nucleotides that modulate PyrR binding to RNA *in vitro* were determined so that these values could be compared with likely intracellular concentrations of the nucleotides. Measurements of the binding of RNA to PyrR over a wide range of nucleotide concentrations in the filter binding assay yielded the concentration at which the effect of the nucleotide was half-maximal (Table 2). As a function of concentration, UMP was ten-fold more effective than UTP at stimulating binding of PyrR to BcBL1 and 100-fold more effective than UTP at stimulating binding to BcBL2. Additionally, the UTP concentration necessary for activation of PyrR was almost ten-fold lower for BcBL1 than for BcBL2. As a function of concentration, GTP was a much more effective inhibitor of RNA binding than GMP. Even though addition of a
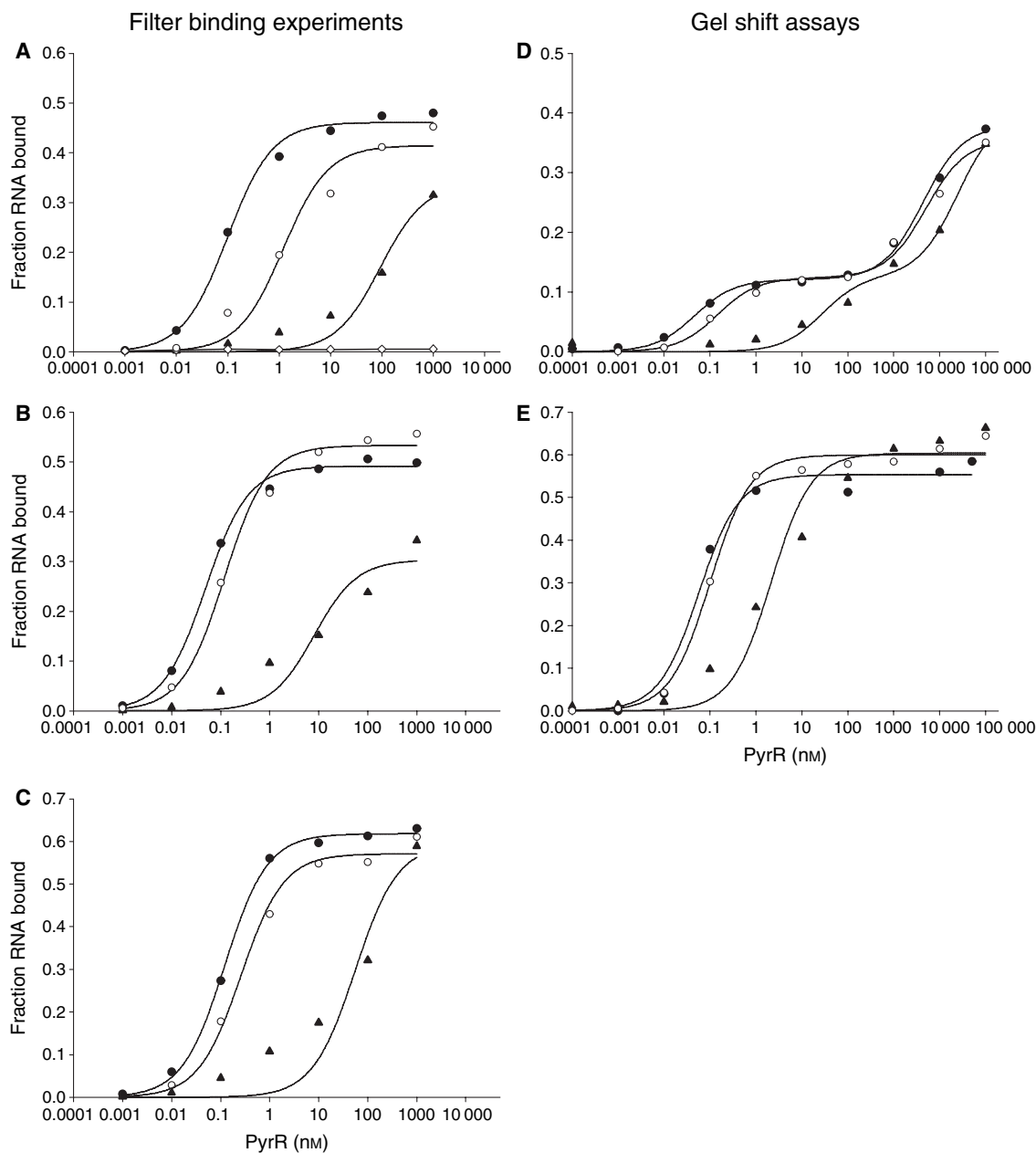
Fig. 2. Representative filter binding experiment of the ^{32}P-labeled PyrR binding loops, BcBL1 (A), BcBL2 (B) and BcBL3 (C), to various concentrations of PyrR in the absence of effector (open circles), with 500 μM UMP (closed circles) or 500 μM GMP (closed triangles). Binding to a control RNA (the antisense strand of BcBL1) is indicated by open diamonds (A). Representative eletrophoretic gel mobility shift assay with ^{32}P-labeled BcBL1 (D) and BcBL2 (E) in the absence of effector (open circles), with 500 μM UMP (closed circles) or 500 μM GMP (closed triangles).

saturating GMP concentration resulted in a higher apparent dissociation constant for RNA than did GTP (Table 1), the concentration required to achieve this inhibition was much higher for GMP (Table 2). The high concentration of GMP needed to affect RNA binding, as compared to GTP, suggests that GTP is the more likely physiological regulator, especially given that nucleoside triphosphate levels are usually several-

fold higher than levels of the corresponding nucleoside monophosphate *in vivo*.

The guanosine to uridine nucleotide ratio governs PyrR binding to *pyr* RNA

Table 3 shows the effects of varying the ratio between effectors that increase and effectors that decrease

Table 1. Apparent RNA dissociation constants (K_d values) from filter binding determinations of PyrR binding to the three *pyr* operon binding loops. The effectors were present at 0.5 mM. The data are averages of at least three independent determinations and include standard deviations of the mean value.

	K_d values (nM)		
	BcBL1	BcBL2	BcBL3
No effector	0.87 ± 0.3	0.13 ± 0.02	0.21 ± 0.08
UMP	0.07 ± 0.02	0.04 ± 0.01	0.08 ± 0.05
UDP	0.07 ± 0.02	0.04 ± 0.01	ND
UTP	0.09 ± 0.02	0.04 ± 0.01	ND
dUMP	0.16 ± 0.08	0.05 ± 0.01	ND
PRPP	0.11 ± 0.03	0.06 ± 0.01	ND
GMP	79 ± 17	5.2 ± 2.9	49 ± 25
GDP	37 ± 12	2.7 ± 1.6	ND
GTP	12 ± 3	1.1 ± 0.2	ND
dGMP	9 ± 5	0.73 ± 0.01	ND

ND, not determined.

Table 2. Half-maximum concentrations of nucleotides or PRPP required for either activation (UMP, UTP and PRPP) or inhibition (GMP and GTP) of binding of PyrR to BcBL1 and BcBL2. Data are the average of at least two independent determinations.

	Half-maximum concentration (μM)	
	BcBL1	BcBL2
UMP	0.04 ± 0.02	0.02 ± 0.01
UTP	0.3 ± 0.2	2.4 ± 0.7
PRPP	0.7 ± 0.3	2.0 ± 1.4
GMP	269 ± 143	232 ± 162
GTP	18 ± 6	8 ± 6

Table 3. Effects of the ratio of guanosine to uridine nucleotide concentrations on binding of PyrR to BcBL2. The total concentration of nucleotides was held constant at 1 mM.

Concentration of nucleotide (μM)		K_d value for RNA (nM)	Concentration of nucleotide (μM)		K_d value for RNA (nM)
GMP	UMP		GTP	UTP	
0	0	0.13	0	0	0.13
0	1000	0.06	0	1000	0.05
100	900	0.06	50	950	0.06
250	750	0.05	150	850	0.09
500	500	0.11	250	750	0.11
750	250	0.29	500	500	0.17
900	100	0.84	750	250	0.40
950	50	1.1	900	100	0.61
1000	0	9.8	1000	0	0.75

Structural requirements of effectors for affecting PyrR binding to BcBL2

To learn more about how PyrR distinguishes purine and pyrimidine nucleotides, we tested the ability of purine and pyrimidine nucleotide structural variants to activate or inhibit binding of BcBL2 to PyrR (see supplementary Table S1). In general, RNA binding to PyrR was activated by pyrimidine nucleotides regardless of structure, whereas the specificity of purine nucleotide effects on RNA binding indicated that both the exocyclic oxo and amino groups of the purine ring and the 2′-hydroxyl group of ribose in GMP contribute significantly to its action. These observations suggest specific interactions between PyrR and the purine ring of purine nucleotides that do not occur with pyrimidine nucleotides, even though such interactions have not been observed in the presently available X-ray structures of PyrR-nucleotide complexes [10,11].

Effects of Mg^{2+}, pH and temperature on binding of PyrR to BcBL2

Experiments characterizing the effects of Mg^{2+} ion concentration, pH and temperature on the binding of BcBL2 RNA to PyrR in the filter binding assay are shown in detail in the Supplementary Material. Three important conclusions were derived from these studies. First, Mg^{2+} ions at a concentration of 10 mM or higher were essential for tight binding of RNA. Inclusion of Mg^{2+} ions in the electrophoresis gel was subsequently found to be crucial for obtaining tight binding of RNA in the gel shift assay. Second, the affinity of PyrR for BcBL2 RNA was 50-fold higher at pH 7.5 than at pH 5.5, and the effect of GMP on RNA binding was strongly pH dependent, whereas the effect of

binding of PyrR to BcBL2 RNA with the total concentration of the two effectors held constant. When the GMP to UMP ratio was increased from 0.11 to 19, the apparent dissociation constant for RNA increased 18-fold, demonstrating the antagonism of the two effectors. When the ratio of GTP to UTP was varied over the same range, the effects were similar to the effects of GMP and UMP; the values for the apparent K_d for BcBL2 varied over a ten-fold range. The effects of PRPP on RNA binding to PyrR were similar to those of uridine nucleotides (Table 1); GMP and GTP also antagonized the effects of PRPP (data not shown), as would be expected if PRPP and the nucleotides bind at the same site. From these observations, we predict that the most important factor regulating the affinity of PyrR for target *pyr* RNA sites *in vivo* is the intracellular ratio of guanosine nucleotides to uridine nucleotides, rather than the concentration of the individual nucleotides.

UMP was much less so (see supplementary Fig. S1A). Ionization of one of four histidine residues in *B. caldolyticus* PyrR may mediate the pH dependence of the GMP effect on RNA binding. Finally, the binding studies in the present study were conducted at 0 °C to ensure stability of the components, for convenience in maintaining a constant temperature, and for comparison with the results of previous gel shift studies. However, an increase in temperature promotes dissociation of a protein–RNA complex; an increase in temperature from 0 °C to 50 °C, which is close to the growth temperature for *B. caldolyticus*, increased the apparent K_d for BcBL2 binding to PyrR by approximately 40-fold to 4.5 ± 0.2 nM (see supplementary Fig. S1B).

Direct comparison of the filter binding and electrophoretic mobility shift methods with BcBL1 and BcBL2

It was desirable to confirm the fundamental conclusions of the preceding RNA filter binding studies using an alternative method. Previous studies [2] of *pyr* RNA binding by *B. subtilis* PyrR used an electrophoretic gel mobility shift method. Some of these prior findings were different from those described for binding of *pyr* RNA by *B. caldolyticus* PyrR (see Discussion). Therefore, it was important to compare directly the two methods for measuring RNA binding. *Bacillus caldolyticus* PyrR and radiolabeled *B. caldolyticus*

BcBL1 and BcBL2 were used for this comparison because *B. subtilis* PyrR cannot be used for the filter binding method due to this protein not being quantitatively retained by hydrophobic filters.

Inclusion of 1 mM Mg^{2+}-acetate in the electrophoresis gel was necessary to observe binding of either BcBL1 or BcBL2 to *B. caldolyticus* PyrR at concentrations up to 100 μM protein, even though 10 mM Mg^{2+} was included in the binding mixture prior to electrophoresis, the electrophoresis buffer contained 1 mM Mg^{2+}, and the gel was subjected to prior electrophoresis for 90 min before loading the samples. With this modification of the previously used method [2], tight binding of *B. caldolyticus* PyrR to BcBL1 and BcBL2 was observed by the gel shift method (Figs 2D,E and 3, Table 4). The binding of BcBL1 to PyrR was clearly resolved into two phases (Fig. 2D), one corresponding to tight binding (K_{d1} in Table 4) and another that was detected only at high concentrations of PyrR, well above those that could be studied in the filter binding studies. The significance of the species observed at PyrR concentrations greatly in excess of those needed to saturate the RNA is questionable because non-specific binding to RNA cannot be excluded. The binding of BcBL2 was described by a single tight binding curve although, in the presence of 0.5 mM GMP, the binding curve was broad and fitted less well to a simple binding equation (Fig. 2E), as was observed on filter binding of BcBL2 under the same conditions (Fig. 2B). In
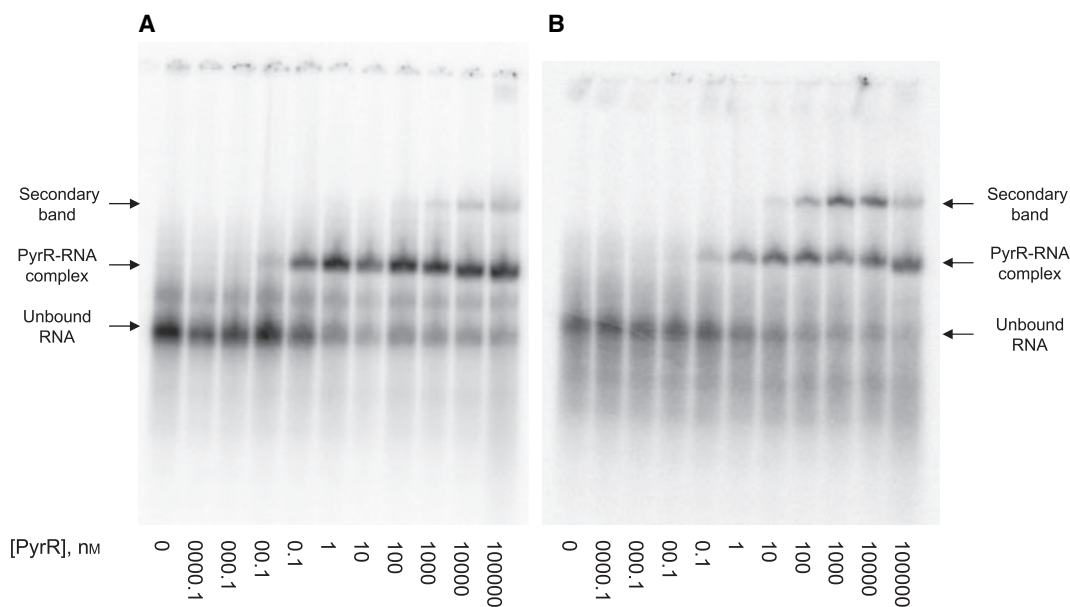

Fig. 3. Analysis of the binding of ^{32}P-labeled BcBL2 to PyrR by the electrophoretic gel mobility shift method in the absence of effector (A) and in the presence of 500 μM GMP (B). The concentration of PyrR (nM subunit) present in each lane is indicated below. The apparent dissociation constants derived from these experiments are shown in Table 4. The presence of the unbound BcBL2 RNA, the PyrR-BcBL2 complex as well as a more slowly migrating secondary band are indicated on the side of each gel.

Table 4. Apparent RNA dissociation constants (K_d values) in electrophoretic gel shift assays of binding of BcBL1 and BcBL2 to PyrR. UMP and GMP were present at 0.5 mM. Data are the average of three to four independent determinations.

	BcBL1		BcBL2
	K_{d1} (nM)	K_{d2} (nM)	K_d (nM)
No effector	0.18 ± 0.04	7650 ± 2500	0.11 ± 0.04
UMP	0.06 ± 0.02	6300 ± 4900	0.07 ± 0.01
GMP	19 ± 8	16800 ± 7400	3.3 ± 1.9

addition, a second, more slowly migrating PyrR-BcBL2 complex was detected at high concentrations of PyrR when 0.5 mM GMP was present (Fig. 3B). In the absence of nucleotide (Fig. 3A) or when 0.5 mM UMP was present (data not shown), this species was barely detectable. Again, the significance of this loosely binding complex is open to question. Importantly, the values for K_d (K_{d1} for BcBL1) and the effects of UMP and GMP (Table 4) agreed reasonably with the corresponding values obtained with the filter binding method (Table 1). We also found that addition of Mg^{2+} to the gel was necessary to obtain tight binding of BcBL2 (K_d = 4 nM) to *B. subtilis* PyrR (data not shown). Thus, if care was taken to include 1 mM Mg^{2+} in the electrophoresis gel, similar results for the tight binding RNA curves were obtained by both methods, a finding that provides confidence in their validity.

Binding of BcBL2 structural variants to PyrR

The binding of RNA to *B. caldolyticus* PyrR exhibits high RNA sequence specificity, as expected from previous genetic and biochemical studies with *B. subtilis* PyrR [2,6]. This was established by filter binding assay of *B. caldolyticus* PyrR to three variants of *B. caldolyticus* BL2 containing single base substitutions (Fig. 1). Analogous variants of *B. subtilis* BL2 were observed in previous gel shift studies with *B. subtilis* PyrR to have very different apparent K_d values relative to native BL2 [2]. With two of the three structural variants tested, the data (see supplementary Table S2) indicated that a single base substitution in a highly conserved portion of the binding loop RNA (G723A) caused reduced binding to PyrR, whereas a substitution in a non-conserved nucleotide (G726A) did not. However, with a third structural variant, A724C, the binding observed by filter binding was much tighter than that detected by the gel mobility shift method (Supplementary material). Binding of this structural variant, however, was clearly altered from the wild-type RNA and

additional experiments indicated that the A724C variant RNA differs from the wild-type BcBL2 in its interaction with Mg^{2+} (Supplementary material).

Effects of uridine and guanosine supplementation on *pyr* gene expression *in vivo*

If PyrR-mediated regulation of the *pyr* operon in *Bacillus* species is largely responsive to the ratio of uridine to guanosine nucleotides, as suggested by the effects of these nucleotides on binding of PyrR to binding loop RNA *in vitro*, then addition of guanosine or uridine to the bacterial growth medium would be expected to stimulate or repress, respectively, the expression of *pyr* genes. Assays of aspartate transcarbamylase (ATCase), the enzyme encoded by *pyrB*, the third cistron of the operon, provided a convenient measure of operon expression in such experiments. Inclusion of guanosine in the growth medium increased the level of ATCase in *B. subtilis* cells by approximately 45% compared to a control culture without supplementation; inclusion of uridine decreased ATCase levels by almost two-fold (Table 5). When both uridine and guanosine were included in the medium in equal amounts, the ATCase level was largely repressed, but expression increased substantially as the ratio of guanosine to uridine was increased. The results demonstrate competition between the effects of guanosine and uridine in the medium. As expected, the effects of nucleoside addition were not observed in a mutant strain of *B. subtilis* [4] in which the *pyrR* gene was deleted. These observations demonstrate that the effects of nucleotides on RNA binding to PyrR *in vitro* correlate with their predicted effects on *pyr* gene expression *in vivo*.

It should be noted that the effects of guanosine on ATCase expression shown in Table 5 were obtained

Table 5. Effects of nucleoside supplementation in the growth medium on the expression of *B. subtilis* ATCase.

Strain	Addition to the medium (µg·mL^{-1})		ATCase specific activity (nmol·min^{-1}·mg^{-1})
	Guanosine	Uridine	
DB104	None	None	86 ± 5
DB104	50	None	120 ± 11
DB104	None	50	56 ± 4
DB104	50	50	47 ± 6
DB104	50	10	110 ± 14
DB104	50	2	130 ± 9
DB104 Δ*pyrR*	None	None	1300 ± 390
DB104 Δ*pyrR*	50	None	1300 ± 390
DB104 Δ*pyrR*	None	50	1400 ± 420

with cells grown with succinate as the carbon source. Similar, but even larger, effects could be observed with glucose-grown cells only in cultures harvested at the end of exponential growth on limiting glucose; if the cells were harvested during growth on excess glucose, the stimulation of ATCase levels by guanosine was not observed, although strong repression by uridine was observed. These results indicate that guanosine uptake and/or conversion to nucleotides is repressed by growth on glucose [15], which masks the effect of guanosine on *pyr* operon expression under such conditions.

Studies of RNA binding to PyrR by analytical ultracentrifugation

The quaternary structure of *B. caldolyticus* PyrR in solution was determined from both sedimentation velocity and equilibrium sedimentation experiments at high and low protein concentrations and in the presence and absence of 0.1 M NaCl. The results of the sedimentation velocity studies are summarized in the (supplementary Table S3). The calculated weight average mass was in the range 83–101 kDa for native PyrR and 94–99 kDa for the His-tagged PyrR used in sedimentation velocity studies of RNA binding described below. The masses calculated from the sequences of the native and His-tagged PyrR in the tetrameric forms are 79.8 and 91.2 kDa, respectively. Since these weight average masses are calculated from the change in shape of moving boundary during the run, and the data are susceptible to various systematic errors, the variation observed in the mass shown in Table S3 is within experimental error.

Data from a sedimentation equilibrium study and an approach to equilibrium analysis of native PyrR over the concentration range of the 0.25–25 μM subunit (see supplementary Figs S3 and S4) fit adequately to sedimentation of a single tetrameric species with a calculated weight average mass of 78.3 kDa, although an alternative fit of the data to a model for sedimentation of a dimeric and tetrameric species in equilibrium could not be excluded (Supplementary material). A similar sedimentation equilibrium study with His-tagged PyrR (0.25–25 μM) provided results similar to native PyrR except that the fitted weight average mass was 91.6 kDa. Altogether, the sedimentation velocity and equilibrium studies show that both native and His-tagged PyrR exist largely as tetramers in solution at concentrations greater than 1 μM, which is in accordance with previous results obtained with size exclusion chromatography and X-ray crystallography [10]. These data and

conclusions are discussed in greater detail in the Supplementary material.

Sedimentation velocity was also used to analyze the binding of RNA to PyrR. Purified His-tagged PyrR was used for these studies because the native PyrR contained traces of ribonuclease, which might have degraded the RNA during the 3-day duration of the titration experiment. As shown in Fig 4A, a 36 nt *pyr* binding loop RNA derived from BcBL2 sedimented as a single RNA species (s20,w = 2.63 S, molecular mass = 12 900 Da) (molecular mass calculated from sequence = 11 600 Da). This BcBL2 sample was titrated by adding aliquots of concentrated PyrR (Fig. 4B–E), so that up to six equivalents of monomer were added without significant dilution (< 7%) of the RNA. Species analysis using either the basic
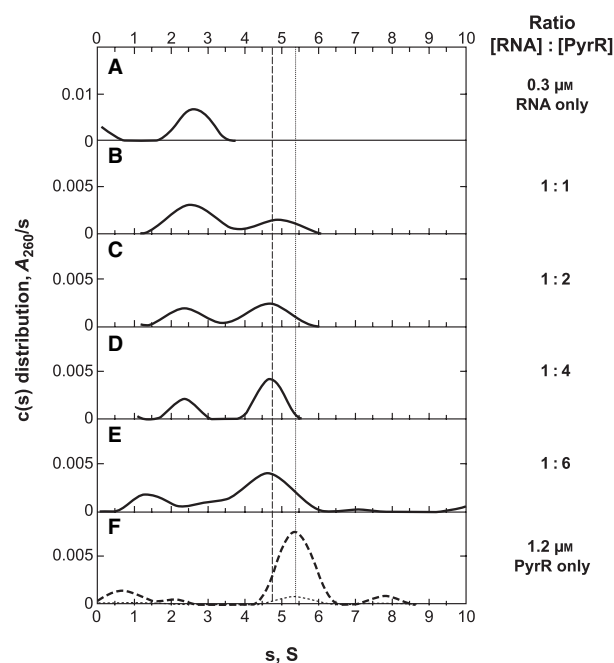

Fig. 4. A size-distribution analysis of sedimenting species observed during a titration of *pyr* binding loop RNA with increasing amounts of PyrR. A plot of c(s) distributions against the uncorrected sedimentation coefficient, s, is shown for RNA only (A), for molar ratios RNA to PyrR subunit (B–E), and for PyrR (F) from absorbance data collected at 260 nm. The c(s) values in the PyrR panel (F) were multiplied by factors of 10 (dotted line) and 100 (dashed line) to make them visible on the same scale as used for the other panels. The initial concentration of RNA was 0.3 μM for (A) and four separate aliquots of PyrR were added to give the final ratios shown. A concentration of PyrR of 1.2 μM was used in (F). The sedimentation distributions, c(s), were calculated using SEDPHAT; 72 scans were collected at 3-min intervals. Further experimental details are given in the Experimental procedures. The vertical dotted line relates the protein peak to the other panels and the vertical dashed line does the same for the PyrR–RNA complex.

non-interacting model of SEDPHAT [16,17] or the more powerful hybrid local continuous distribution/global discrete species model [16,17] showed that only two sedimenting species were present at significant concentrations in the range of 0.1–5 S for each aliquot added (see supplementary Table S4). The first of these (s20,w = 2.6 S) corresponds to the free RNA. A second species appeared (s20,w = 4.9 S) that must correspond to an RNA–PyrR complex because added PyrR will not contribute more than 1–2% to the total 260 nm absorbance at the concentrations added. On titrating the RNA with increasing amounts of PyrR, the loading concentration of the peak corresponding to free RNA declined, and that for the second peak increased, as shown by the area under the peaks in the c(s) distribution shown in Fig. 4. An additional shoulder at ∼ 3 S, whose shape and position are somewhat variable, is evident in Fig. 4E (see supplementary Fig. S5), where the protein concentration is approximately three-fold greater than that necessary to saturate the RNA with the PyrR dimer. Based on the species analysis above, we strongly suspect that this shoulder is an artifact that results from the sensitivity of the c(s) distribution to boundary effects. As with the filter binding assays, some of the RNA (∼ 30%) remained unbound at greater than saturating concentrations of PyrR. In Fig 4F, the PyrR stock solution was diluted to 1.2 μM subunits into the same buffer and centrifuged under the same conditions as used for the other panels in Fig. 4. Most of the protein sedimented as a tetramer with an s20,w = 5.5 S with a minor species at approximately 10% of the tetramer concentration with an s20,w = 2.3 S and an estimated molecular mass of 18 000 Da, which is likely a nonparticipating PyrR monomer (sequence molecular mass = 22 800 Da). The sedimentation coefficients and buoyant mass variation observed with increasing PyrR concentrations are summarized in the (supplementary Table S4). The s values in Table S4 for the free RNA peak decreased significantly with increasing PyrR concentration. We demonstrated that the *pyr* RNA appeared to be electrophoretically intact following the 3-day experiment at 20 °C (data not shown), so the decrease in s value for the RNA is not the result of RNA degradation. The sedimentation coefficient of the new species (4.6–4.9 S) is significantly lower than that of free PyrR (5.4 S); a complex of RNA with the PyrR tetramer would be expected to have a larger s value than free PyrR, barring a large, unexpected increase in the hydrodynamic radius. Thus, the complex of RNA with PyrR must involve association with the protein in a form smaller than the tetramer. If the buoyant mass of the RNA is

subtracted from that of the complex and the molecular weight of the remaining protein calculated, using a partial specific volume of 0.74 (determined from the amino acid composition of PyrR) and a solvent density of 1.0 g·mL^{-1}, the value obtained is 37 100 for the protein component. This is in reasonable agreement with the mass of a His-tagged PyrR dimer (44 000). Finally, Fig. 5 shows a plot of the free RNA remaining against the ratio of PyrR subunit concentration to the initial RNA concentration (see supplementary, Table S4). The trend in the data is that of a typical stoichiometry plot where the RNA concentration is in large excess of its dissociation constant for PyrR. The data are consistent with a stoichiometry of one RNA molecule per PyrR dimer in the complex with approximately 30% of the RNA that does not bind under these conditions. Thus, we conclude that the complex has the composition of (PyrR)$_2$-RNA.
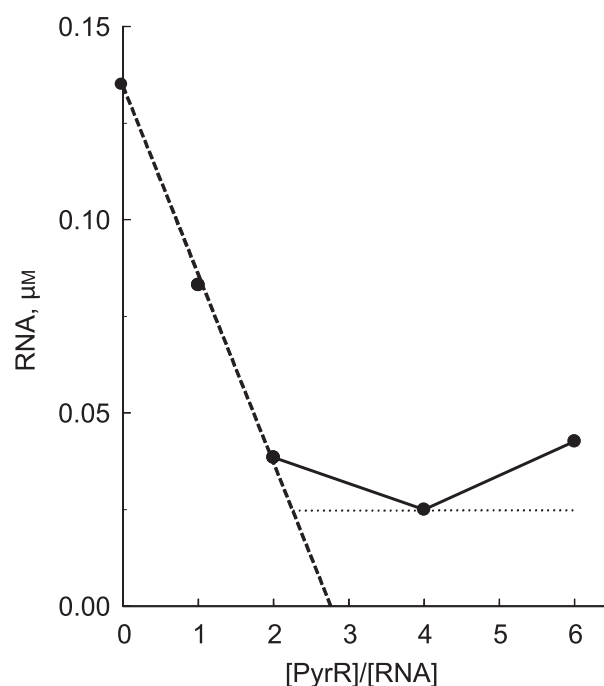

Fig. 5. A plot of A_{260} for the free RNA peak, which is obtained by integrating the area under the peak in the s range of 2–2.6 S, against the molar ratio of PyrR to RNA in the sample. The data were obtained from the analytical ultracentrifugation experiment described in Fig. 4. The free RNA values were corrected for a slight loss of total A_{260} in the range 5–20%, of which a maximum of 5% was due to dilution. The dotted line shows a least-squares fit through the first three points. The horizontal dotted line shows the concentration of non-binding RNA from Fig. 4D, in which the RNA peak is clearly defined. The intersection between the dashed and dotted lines indicates that two subunits of PyrR bind to one RNA stem-loop.

Discussion

Complexity of RNA binding to PyrR

The complex binding curves for BcBL1 and for all three binding loop RNAs in the presence of guanosine nucleotides (Fig. 2) indicate that the binding of RNA to PyrR cannot be fully described by a simple binding equilibrium. Although the biophysical basis for the complexity of the RNA binding curves is not established, we suggest that it arises from multiple PyrR conformational and/or aggregation states that differ in their affinity for RNA and possibly also for nucleotides. PyrR conformation is implicated because the heterogeneity in RNA binding is strongly affected by uridine and guanosine nucleotides, which are known to bind to the UPRTase active site of PyrR [10]. The simplest model that fits our observations posits the existence of two PyrR conformations, with one having a higher affinity for RNA than the other. The high affinity state is favored by binding of either uridine nucleotides or binding of RNA itself in the case of BcBL1. The low affinity state is favored by the binding of guanosine nucleotides. Thus, RNA binding involves at least two coupled reactions: RNA binding to PyrR and nucleotide binding to PyrR.

The demonstration by analytical ultracentrifugation that the PyrR tetramer dissociates into dimers when RNA binds adds yet another reaction that is likely coupled to the RNA and nucleotide binding reactions discussed above. It is likely that, at high dilution, tetrameric PyrR dissociates to dimers in the absence of RNA, but this could not be conclusively demonstrated at the lowest concentration (1 μM) that could be analyzed by analytical ultracentrifugation. We note, however, that all of the filter binding experiments were conducted at PyrR concentrations well below this value, where some or all of the PyrR may be present in dimeric form. We propose that the tetrameric form of PyrR has low affinity for RNA because the likely RNA binding site is known from the crystal structures to be occluded in the center of the tetramer [10,11]. The dimeric form of PyrR, in which the RNA binding site would be exposed to the solvent, is likely to have higher affinity for RNA. Coupling of the dimer–tetramer equilibrium to the equilibria for PyrR–RNA binding and PyrR–nucleotide binding could explain the complex binding curves observed in the present study, especially when RNA binding in the presence of guanosine nucleotides was examined.

The involvement of multiple coupled equilibria (i.e. PyrR tetramer–dimer association together with binding of RNA and nucleotides to dimer and tetramer with different affinities for each state of aggregation) in the experimentally observed RNA binding in the present study dictates that one should not regard the apparent K_d values for RNA or the half-maximal values for nucleotide effects on RNA binding as simple equilibrium constants. Hence, we have consistently used the term 'apparent K_d' to describe the concentrations of PyrR that yielded half-maximal RNA binding in our experiments.

Correlations between results of filter binding studies and electrophoretic mobility shift studies of RNA binding

Direct comparison of the binding of BcBL1 and BcBL2 to *B. caldolyticus* PyrR by the filter binding and gel shift methods demonstrated that, as long as Mg^{2+} was included in the electrophoresis gel, there was good agreement between the two methods. However, agreement was much poorer with the A724C structural variant of BcBL2 RNA, even with a high Mg^{2+} concentration in the gel. The sensitivity to Mg^{2+} and to the structure of the RNA studied suggests that the gel shift method can give highly misleading results in some cases. An RNA that dissociates rapidly from PyrR may appear to bind poorly, or not to bind at all, in the gel shift assay. We conclude that, for protein–RNA binding studies in general, it would be prudent to confirm electrophoretic mobility shift conclusions whenever possible by an alternative method, such as a filter binding assay.

In light of our current observations on the importance of Mg^{2+} in gel shift assays with PyrR and *pyr* binding loop RNAs, the studies of the specificity of RNA binding of *B. subtilis* PyrR should be re-examined. Our findings with the native and the G723A and G726A sequence variants of BcBL2 indicate that the effects on affinity observed previously for native BsBL2 and its structural variants [2] are valid, at least qualitatively. However, previous observations indicating that *B. subtilis* PyrR binding to BsBL1 and BsBL3 was weak and barely affected by uridine nucleotides are misleading and probably resulted from the dissociation of the required cation Mg^{2+} from these two RNAs, but not BsBL2, during electrophoresis. We now have evidence that PyrR from both *Bacillus* species binds tightly to all three binding loop RNAs from both species and that binding of all three RNAs is significantly modulated by nucleotides (data not shown).

Physiological implications of these studies

The data provided in Tables 1–3 indicate that uridine nucleotides and guanosine nucleotides are the primary

metabolite modulators of PyrR binding to *pyr* attenuator region RNA, and hence the primary regulators of pyrimidine biosynthesis. Uridine nucleotide stimulation of RNA binding is easily understood in terms of feedback regulation (i.e. end-product repression of the *pyr* operon) because binding of PyrR to RNA leads to increased termination of transcription prior to transcription of *pyr* genes coding for biosynthetic enzymes. UMP and UTP exert their effects on RNA binding *in vitro* in the micromolar concentration range, well below their estimated concentrations in exponentially growing cells (i.e. 1 mM for UTP and 0.1–0.3 mM for UMP) [18]. GTP is probably the primary physiological guanosine nucleotide modulator because it is effective at a much lower concentration than GMP (Table 2) and is present in growing cells at approximately 0.6 mM [19], well above the concentrations at which it exerts its effects on RNA binding to PyrR. The effects of GMP are unlikely to be significant *in vivo* because intracellular GMP levels [19,20] do not reach the concentration required to antagonize RNA binding.

Of the other metabolites studied, none appears as being likely to serve as a physiologically important modulator of *pyr* operon expression. In particular, in previous publications [4,9], we suggested that PRPP might may be a feed-forward regulator because it would be expected to compete at uridine nucleotide binding sites. However, the data obtained in the present study indicate that PRPP actually behaves like UMP and UTP to stimulate RNA binding to PyrR. PRPP also fails to antagonize the effects of GTP on RNA binding nearly as effectively as UMP or UTP (data not shown). Thus, the effects of PRPP do not appear to be physiologically important in the regulation of *pyr* expression.

The intracellular concentrations of uridine nucleotides exceed the half-maximal concentrations required for activation of PyrR binding to RNA by two or three orders of magnitude (Table 2), even allowing for an increase of up to 40-fold in the K_d values for PyrR binding to RNA measured at 0 °C when shifted to the physiological growth temperature for *B. caldolyticus* (see supplementary Fig. S1B). The values of the apparent dissociation constants suggest that PyrR functions as a regulator of *pyr* gene expression largely under conditions where the affinity of PyrR for *pyr* attenuator sites is substantially reduced by the antagonistic effect of guanosine nucleotides. Because guanosine and uridine nucleotides can compete for binding to the same sites on PyrR [10], the affinity of the protein for *pyr* RNA will be determined by the ratio of their intracellular concentrations, and not by the concentration of the individual nucleotides. Table 3 illustrates how

the affinity of PyrR for BcBL2 RNA varied over a ten- to 20-fold range as a function of the GMP/UMP or GTP/UTP ratios. The experiments in Table 3 were conducted at a total nucleotide concentration of 1 mM, which is near their physiological concentration and well above the concentrations at which the individual nucleotides exert their effects on RNA binding. Most importantly, investigations of the effects of nucleoside addition to the growth medium on *B. subtilis pyrB* (ATCase) expression *in vivo* (Table 5) support the conclusion that the ratio of guanosine to uridine nucleotides dominates PyrR action. The crucial role of guanosine nucleotides in the regulation of *pyr* genes in bacilli was not fully appreciated before these studies were conducted.

The cross-regulation of pyrimidine biosynthesis by guanosine nucleotides is part of a more general phenomenon. The accumulation of high levels of intracellular guanosine nucleotides indicates that cells have adequate carbon, nitrogen and energy sources for RNA and DNA synthesis. Thus, accumulated purine nucleotides constitute appropriate feed-forward metabolites to stimulate pyrimidine nucleotide biosynthesis. Other examples of such feed-forward activation of pyrimidine biosynthesis in *Bacillus* species include the activation by GTP of the pyrimidine-repressible carbamyl phosphate synthetase [21], of UMP kinase [22] and of CTP synthetase [23]. Furthermore, GTP levels are used as regulatory signals governing a variety of more global regulatory circuits in *Bacillus* cells. Examples of this regulatory function of the GTP pool in *B. subtilis* include the regulation of ribosomal RNA synthesis [24], initiation of sporulation [25], activation of the CodY regulon in nutrient-starved cells [26], and conversion of GTP to ppGpp and pppGpp during the stringent response to amino acid starvation [25]. A reduction in intracellular GTP without a corresponding decline in uridine nucleotide pools would result in much tighter binding of PyrR to attenuation region RNA and reduced expression of the *pyr* operon, which is an appropriate response to the original nutrient limitation.

Experimental procedures

In vitro transcription and purification of ^{32}P-labeled RNA

For synthesis of radiolabeled RNA by *in vitro* transcription, plasmids containing templates that contained the T7 RNA polymerase promoter followed by DNA specifying one of the three PyrR binding loops (BcBL1, BcBL2 and BcBL3) from the *B. caldolyticus pyr* operon were constructed. The isolated plasmids were used as templates in

PCR reactions to generate products of approximately 150 bp in length that were used as templates for *in vitro* transcription with T7 RNA polymerase. The PCR templates were purified using the GFX purification kit prior to *in vitro* transcription using the MaxiScript kit from Ambion (Austin, TX, USA). The procedure recommended by the manufacturer was used, except that the reactions were incubated for 2 h at 37 °C, and the RNA was labeled by including 10 μM [α-^{32}P]GTP (800 Ci·mmol^{-1}; MP Biomedicals Inc., Irvine, CA, USA) in the reaction mix together with 500 μM of each of ATP, UTP and CTP. Unincorporated nucleotides were separated by running the sample through a G-50 Micro Column from Amersham Biosciences/GE Healthcare (Piscataway, NJ, USA). The labeled RNA was purified using denaturing (8 M urea) 15% polyacrylamide gel electrophoresis as described previously [10]. Following phenol extraction of RNA eluted from a cut-out piece of gel, the RNA was precipitated over night at −20 °C with 1 μg of yeast tRNA as carrier RNA and resuspended in 200 μL buffer (25 mM Tris-acetate pH 7.5, 50 mM K-acetate and 1 mM EDTA). The concentration of the RNA was determined by duplicate liquid scintillation counting of a 10-fold dilution of the RNA sample. Prior to use, the labeled RNA was denatured at 85 °C for 15 min and allowed to refold for 15 min at 37 °C, after which Mg-acetate was added to a final concentration of 10 mM.

Filter binding assays of RNA binding to PyrR

A double-filter method for filter binding [14] was used as described previously [10]. Unless noted otherwise, the reaction mixture contained 25 mM Tris-acetate (pH 7.5), 50 mM K-acetate, 10 mM Mg-acetate, 25 pM ^{32}P-labeled RNA, 0.04 U·μL^{-1} of RNase inhibitor (Superase-In; Ambion), 100 μg·mL^{-1} (~ 4 μM) of yeast tRNA, 50 μg·mL^{-1} of acetylated BSA, nucleotides at the indicated concentrations and various concentrations of native *B. caldolyticus* PyrR, which was purified as described previously [10]. The concentration of the PyrR protein was determined using the Bradford assay obtained from Bio-Rad (Hercules, CA. USA). The 50 μL reaction mixtures were allowed to incubate for 40 min on ice prior to filtering through the two membranes followed by a single wash with 50 μL of binding buffer. Filtration and washing were complete within 60 s. For some experiments, the pH was varied by use of a 25 mM Tris-25 mM 2-(*N*-morpholino)ethanesulfonate-acetate buffer. For experiments where the temperature was varied, the pH of binding buffer was adjusted at each temperature examined to the pH of binding buffer at room temperature. The filters and the washing buffer were all equilibrated at the relevant temperature for at least 30 min prior to the experiments and the filtration apparatus was used at the temperature indicated. After overnight exposure of the membranes to a PhosphorImager screen, the radioactivity was determined using a PhosphorImager and quanti-

fied using IMAGEQUANT software (Molecular Dynamics/GE Healthcare, Sunnyvale, CA, USA). Dissociation constants were determined by fitting the data to a simple binding equation using SIGMAPLOT 9.0 (Systat Software, Inc.. San Jose, CA, USA) as described previously [10] or, when two phases were clearly identified, to a two-state binding curve. Since the RNA concentration of 25 pM was close in some cases to the apparent K_d, these data were also fitted to a quadratic binding equation [27], but the calculated apparent K_d values obtained were not significantly different from those obtained with the simple binding equation. To determine the concentration of nucleotides required for half-maximum effect on PyrR binding to the RNA, the obtained K_d values from at least two independent experiments were plotted against the nucleotide concentration, and the half-maximum concentration and standard deviation were calculated by SIGMAPLOT 9.0. Only approximately 50–60% of the total radioactive RNA was bound by saturating levels of PyrR; this was consistently observed for all three binding loop RNAs (Fig. 2) and a similar result was noted in sedimentation velocity experiments. We suggest that the unbound RNA consists of species that do not fold into the native secondary structure required for binding.

Electrophoretic gel mobility shift assays of RNA binding to PyrR

Gel shift analysis was performed essentially as described previously [2] with the following modifications. The gels were run in a Bio-Rad Protean IIxi apparatus cooled to 4 °C and contained 6% acrylamide (37.5 : 1 acrylamide/bis solution), 12.5 mM Tris-acetate (pH 7.5), 2.5% glycerol and 1 mM Mg-acetate. The running buffer contained 12.5 mM Tris-acetate (pH 7.5) and 1 mM Mg-acetate. The gels were pre-run for 1.5 h at 150 V followed immediately by loading of 15 μL of sample, electrophoresis for 15 min at 50 V and for 3 h at 300 V. After electrophoresis, the gels were dried on filter paper and exposed overnight to a PhosphorImager screen. Data were analyzed as described above. The RNA binding mixture (50 μL) used for gel shifts was the same as that employed in the the filter binding experiments, except that BSA was omitted and 0.0125% loading dye (xylene cyanol) and 5% glycerol were added. Binding of RNA to appreciably higher concentrations of PyrR could be better characterized by the gel shift method than by the filter binding method described above because concentrations of PyrR in excess of 1 μM were not quantitatively retained by the nitrocellulose filter.

Preparation of ribonuclease-free PyrR for analytical ultracentrifugation

His-tagged *B. caldolyticus* PyrR was used in the ultracentrifugation experiments. Direct comparison of the binding

of BcBL2 RNA to His-tagged PyrR and to native PyrR under identical conditions by the filter binding methods demonstrated that binding of RNA to His-tagged PyrR was modulated by nucleotides in the same manner as native PyrR, but the apparent K_d for RNA was approximately 100-fold larger. For preparation of His-tagged PyrR, the PyrR coding sequence was amplified from pSHCO2, a plasmid containing *B. caldolyticus* PyrR [10], and ligated into plasmid pET412b, which is a pET41 derivative encoding a C-terminal octa-histidine tag preceded by the cleavage site for tobacco etch virus protease (E. Harms, Purdue University, Lafayette, IN, USA, personal communication); the resultant plasmid is pCalCHIS. *Escherichia coli* strain BL21-DE3 was transformed with pCalCHIS for *pyrR* expression. Cultures of *E. coli* BL21-DE3/pCalCHIS were grown in LB medium at 37 °C until an absorbance of 0.8 was reached at A_{600}, induced with 0.4 mM isopropyl thio-β-D-galactoside and grown for 4 h at 37 °C. Cells were harvested and lysed by sonication in buffer containing 20 mM Tris (pH 7.5), 500 mM NaCl. The lysate was centrifuged at 25 000 *g* at 4 °C for 30 min. Because PyrR at high concentration is insoluble in the high-salt buffers used for Ni-affinity purification, the purification protocol employed high ionic strength prior to elution, and low ionic strength during elution. Following filtration through a 0.4 μm membrane, the supernatant was batch-bound to Ni-Sepharose resin (Amersham) in buffer containing 20 mM Tris (pH 7.5), 500 mM NaCl supplemented with 100 mM imidazole to minimize binding of *E. coli* proteins. The resin was washed in 20 mM Tris (pH 7.5) and 100 mM imidazole, packed into a Bio-Rad Econo-Column and eluted in 20 mM Tris (pH 7.5) with a 0.1–1.0 M imidazole gradient. The protein eluted at approximately 600 mM imidazole. Fractions were pooled and dialyzed against 20 mM Tris (pH 7.5), 5% glycerol. Remaining traces of RNase contaminants were by chromatography of purified PyrR on an Amersham Superdex 200 HiLoad16/60 column, eluting with 0.1 M Tris-HCl (pH 7.5) and 0.15 M NaCl. The pooled fractions were dialyzed against buffer containing 20 mM Tris (pH 7.5). The RNase-free status of purified PyrR was confirmed by detection of no degraded RNA species on gel electrophoresis of samples that had been incubated with radiolabeled RNA for 2 weeks at room temperature.

Analytical ultracentrifugation

Sedimentation equilibrium and velocity experiments using either native PyrR or His-tagged PyrR were run on a Beckman XL-I Analytical Ultracentrifuge (Beckman-Coulter, Fullerton, CA, USA) at 20 °C. Carbon filled epon two sector centerpieces and sapphire windows were used for all experiments. In all experiments, a buffer of 20 mM Tris-Cl (pH 7.5) and, in some cases, 10 mM $MgCl_2$ and 0.1 M NaCl were included. The cell and rotor were equilibrated under vacuum and at 0 r.p.m. for at least 1 h prior to the start of

the run so that the system could reach thermal equilibrium. For the velocity experiments, the centrifuge was started from 0 r.p.m. and data collection began immediately with scans collected every 3 min. Both absorbance and interference data were usually collected. For the equilibrium experiments, both approach to equilibrium data and data at equilibrium were collected and the samples were pre-equilibrated as described above. The condition of equilibrium was tested using the program WINMATCH 0.99 from the RASMB software archive (http://www.rasmb.bbri.org/rasmb). The sample took 40 h to initially reach equilibrium and 24 h between speed changes.

Multiwavelength sedimentation velocity experiments were undertaken to define the stoichiometry of the RNA–PyrR complex in solution. However, only data obtained at 260 nm had sufficient signal to noise ratio to be used for the entire range of the titration. His-tagged PyrR was prepared by dialysis against buffer containing 20 mM Tris-Cl (pH 7.5), 10 mM $MgCl_2$. BcBL2 RNA (nucleotides 702–737; Fig. 1B), which was chemically synthesized by Integrated DNA Technologies (Coralville, IA, USA), was prepared in the same buffer. These experiments were run in a Beckman Optima XL-I ultracentrifuge. A 12 mm path length cell containing a double-sector carbon-filled epon centerpiece with sapphire windows was used for all experiments, and this cell was treated with RNase*ZAP* (Ambion) for 24 h to remove nucleases. The reference and sample sectors were filled with 400 μL of dialysis buffer and sample, containing 0.3 μM RNA, respectively. After thermal equilibration of the sample (at 20 °C for at least 1 h at 0 r.p.m.), all sedimentation velocity experiments were run at 50 000 r.p.m. at 20 °C and scans were recorded at 3-min intervals using both absorbance (at 278 nm and 260 nm) and interference optics.

The initial sedimentation velocity analysis contained only 0.3 μM RNA, which has a calculated molecular mass of 11 564 Da. Immediately after completion of this first experiment, a 5 μL aliquot of dialysis buffer was added to the reference sector, and a 5 μL aliquot of concentrated PyrR protein added to the RNA in the sample chamber. This equimolar mix of PyrR subunit to RNA was sedimented as well. Subsequent sedimentation velocity analyses were performed by titrating the RNA with increasing amounts of PyrR in varying molar ratios. The total time of the binding experiment was 3 days. A final experiment was run in the absence of added RNA at a PyrR subunit concentration of 1.2 μM.

Data were considered to be fitted when plots of the fitting residuals were observed to be evenly distributed around zero and the rmsd was lower than the signal to noise determined from the plateau region of the first scan. Data were usually analyzed using the hybrid local continuous/global discrete model [16] with zero to three discrete species included. For all discrete species, the buoyant mass was calculated, so that masses from molecules with dissimilar partial specific volumes (protein and RNA) would be additive. PyrR has no tryptophan residues and, at the concentrations

used in these experiments (A_{280} and A_{260}) would be no more than 0.0075 AU at the highest protein concentration (1.8 μM).

Solvent densities and viscosities were calculated to be 1.00 g·mL^{-1}A and 0.01 poise, respectively, for the Tris buffer and 1.0039 g·mL^{-1} and 0.01 poise for the NaCl-containing buffer using SEDNTERP [28]. A partial specific volume of 0.7398 cm^3·g^{-1} was also calculated with SEDNTERP from the sequence of His-tagged PyrR and a partial specific volume of 0.7450 cm^3·g^{-1} was calculated from the sequence of the native protein; an approximate value for RNA (0.51 cm^3·g^{-1}) was obtained from Table 2 of Durchschlag and Zipper [29]. The data were fitted to various models using the appropriate algorithms in SEDFIT 9.3b [30] and SEDPHAT 4.1b [16] (obtained from http://www.analyticalultracentrifugation.com).

Growth of *B. subtilis* cells and ATCase assay

To investigate the effects of supplementation of the growth medium with nucleosides on ATCase levels in *B. subtilis*, cultures strains DB104 and DB104*ΔpyrR* [4] were grown on buffered minimal medium [5], which included 0.1% (w/v) casamino acids (Becton Dickinson/Difco, Franklin Lakes, NJ, USA), 50 mg·mL^{-1} histidine and 6 mg·mL^{-1} disodium succinate, supplemented with nucleosides as shown in Table 5. Cells were grown at 37 °C with aeration, harvested in the exponential growth phase by centrifugation, and ruptured by sonication. Cell debris was removed by a 10 min centrifugation (14 000 *g*) and the supernatant was used in assays.

ATCase activity was determined by a radiometric procedure [31]. Assays were performed at 30 °C in a 100 μL final volume containing the following: 50 mM Tris-acetate (pH 8.3), 50 mM [^{14}C]-aspartate (final specific activity of 10 μCi·mmol^{-1}; Amersham), and 10 mM carbamoyl phosphate (Sigma, St Louis, MO, USA). Reactions were initiated by addition of enzyme and stopped with 900 μL 0.2 M acetic acid after 30 min. A 950 μL portion of each reaction was added to a column containing Dowex AG-50W-X8 (200–400 mesh hydrogen form; Bio-Rad) to retain unreacted aspartate. Columns were washed four times with 400 μL 0.2 M acetic acid with the eluate collected in scintillation vials. Aquasol-2 (Packard Research/Perkin-Elmer, Meriden, CT, USA) was added to the collected eluate, total counts were determined using liquid scintillation counting and used to calculate ATCase activity. Protein concentrations were determined using the BCA protein assay kit (Pierce, Rockford, IL, USA), using BSA as the protein standard.

Acknowledgements

References

1 Switzer RL, Turner RJ & Lu Y (1999) Regulation of the *Bacillus subtilis* pyrimidine biosynthetic operon by transcriptional attenuation: control of gene expression by an mRNA-binding protein. *Prog Nucl Acids Res Mol Biol* **62**, 329–367.

2 Bonner ER, D'Elia JN, Billips BK & Switzer RL (2001) Molecular recognition of *pyr* mRNA by the *Bacillus subtilis* attenuation regulatory protein PyrR. *Nucleic Acids Res* **29**, 4851–4865.

3 Turner RJ, Bonner ER, Grabner GK & Switzer RL (1998) Purification and characterization of *Bacillus subtilis* PyrR, a bifunctional *pyr* mRNA-binding attenuation protein/uracil phosphoribosyltransferase. *J Biol Chem* **273**, 5932–5938.

4 Turner RJ, Lu Y. & Switzer RL (1994) Regulation of the *Bacillus subtilis* pyrimidine biosynthetic (*pyr*) gene cluster by an autogenous transcriptional attenuation mechanism. *J Bacteriol* **176**, 3708–3722.

5 Lu Y, Turner RJ & Switzer RL (1995) Roles of the three transcriptional attenuators of the *Bacillus subtilis* pyrimidine biosynthetic operon in the regulation of its expression. *J Bacteriol* **177**, 1315–1325.

6 Ghim S-Y & Switzer RL (1996) Characterization of *cis*-acting mutations in the first attenuator region of the *B. subtilis pyr* operon that are defective in regulation of expression by pyrimidines. *J Bacteriol* **178**, 2351–2355.

7 Ghim S-Y & Switzer RL (1996) Mutations in *B. subtilis* PyrR, the *pyr* regulatory protein with defects in regulation by pyrimidines. *FEMS Microbiol Lett* **137**, 13–18.

8 Tomchick DR, Turner RJ, Switzer RL & Smith JL (1998) Adaptation of an enzyme to regulatory function: structure of *Bacillus subtilis* PyrR, a bifunctional *pyr* RNA-binding attenuation protein and uracil phosphoribosyltransferase. *Structure* **6**, 337–350.

9 Lu Y & Switzer RL (1996) Transcriptional attenuation of the *Bacillus subtilis pyr* operon by the PyrR regulatory protein and uridine nucleotides in vitro. *J Bacteriol* **178**, 7206–7211.

10 Chander P, Halbig KM, Miller JK, Fields CJ, Bonner HKS, Grabner GK, Switzer RL & Smith JL (2005) Structure of the nucleotide complex of PyrR, the *pyr* attenuation protein from *Bacillus caldolyticus*, suggests dual regulation by pyrimidine and purine nucleotides. *J Bacteriol* **187**, 1773–1782.

11 Chander P (2006) *Structural analysis of the regulatory protein of pyrimidine biosynthesis, PyrR*. PhD Thesis, Purdue University, West Lafayette, IN.

12 Ghim S-Y, Nielsen P & Neuhard J (1994) Molecular characterization of pyrimidine biosynthesis genes from

the thermophile *Bacillus caldolyticus*. *J Gen Microbiol* **140**, 479–491.

13 Ghim S-Y & Neuhard J (1994) The pyrimidine biosynthesis operon of the thermophile *Bacillus caldolyticus* includes genes for uracil phosphoribosyltransferase and uracil permease. *J Bacteriol* **176**, 3698–3707.

14 Wong L & Lohmann TM (1993) A double-filter method for nitrocellulose-filter binding: application to protein-nucleic acid interactions. *Proc Nat Acad Sci USA* **90**, 5428–5432.

15 Schuch R, Garibian A, Saxild HH, Piggot PJ & Nygaard P (1999) Nucleosides as a carbon source in *Bacillus subtilis*: characterization of the *drm-pupG* operon. *Microbiology (Reading)* **145**, 2957–2966.

16 Schuck P. (2003) On the analysis of protein self-association by sedimentation velocity analytical ultracentrifugation. *Anal Biochem* **320**, 104–124.

17 Balbo A, Minor KH, Velikovsky CA, Mariuzza RA, Peterson CB & Schuck P (2005) Studying multiprotein complexes by multisignal sedimentation velocity analytical ultracentrifugation. *Proc Nat Acad Sci USA* **102**, 81–86.

18 Møllgaard H & Neuhard J (1978) Deoxycytidylate deaminase from *Bacillus subtilis*. *J Biol Chem* **253**, 3536–3542.

19 Saxild HH & Nygaard P (1991) Regulation of levels of purine biosynthetic enzymes in *Bacillus subtilis*: effects of changing purine nucleotide pools. *J Gen Microbiol* **137**, 2387–2394.

20 Bernlohr DA & Switzer RL (1983) Regulation of *Bacillus subtilis* glutamine phosphoribosylpyrophosphate amidotransferase inactivation *in vivo*. *J Bacteriol* **153**, 937–949.

21 Paulus TJ & Switzer RL (1979) Synthesis and inactivation of the carbamyl phosphate synthetase isozymes of *Bacillus subtilis* during growth and sporulation. *J Bacteriol* **140**, 769–773.

22 Gagyi C, Burcurenci N, Sirbu O, Labesse G, Ionescu M, Ofiteru A, Assairi L, Landais S, Danchin A, Barzu O *et al.* (2003) UMP kinase from the Gram-positive bacterium *Bacillus subtilis* is strongly dependent on GTP for optimal activity. *Eur J Biochem* **270**, 3196–3204.

23 Willemöes M & Sigurskjold BW (2002) Steady-state kinetics of the glutaminase reaction of CTP synthase from *Lactococcus lactis*. the role of the allosteric activator GTP in coupling between glutamine hydrolysis and CTP synthesis. *Eur J Biochem* **19**, 4772–4779.

24 Krasny L & Gourse RL (2004) An alternative strategy for bacteria ribosome synthesis: *Bacillus subtilis* rRNA transcription regulation. *EMBO J* **23**, 4473–4483.

25 Lopez JM, Dromerick A & Freese E (1981) Response of guanosine 5'-triphosphate concentration to nutritional changes and its significance for *Bacillus subtilis* sporulation. *J Bacteriol* **146**, 605–613.

26 Ratnayake-Lecamwasam M, Serror P, Wong KW & Sonenshein AL (2001) *Bacillus subtilis* CodY represses early-stationary-phase genes by sensing GTP levels. *Genes Dav* **15**, 1093–1103.

27 Schaak JE, Yakhnin H, Bevilqcqua PC & Babitzke P (2003) A Mg^{2+}-dependent RNA tertiary structure forms in the *Bacillus subtilis* trp operon leader transcript and appears to interfere with *trpE* translation control by inhibiting TRAP binding. *J Mol Biol* **332**, 555–574.

28 Laue TM, Shah BD, Ridgeway TM & Pelletier SL (1992) Computer-aided interpretation of analytical sedimentation data for proteins. In *Analytical Ultracentrifugation in Biochemistry and Polymer Science* (Harding SE, Rowe AJ & Horton JC eds), pp. 90–125. The Royal Society of Chemistry, Cambridge, UK.

29 Durschlag H & Zipper P (1997) Calculation of partial specific volumes and other volumetric properties of small molecules and polymers. *J Appl Cryst* **30**, 803–807.

30 Schuck P (2000) Size distribution analysis of macromolecules by sedimentation velocity ultracentrifugation and Lamm equation modeling. *Biophys J* **78**, 1606–1619.

31 Perbal B & Herve G (1972) Biosynthesis of *Escherichia coli* aspartate transcarbamylase I. parameters of gene expression and sequential biosynthesis of the subunits. *J Mol Biol* **70**, 511–529.

32 Zuker M (2003) Mfold web server for nucleic acid folding and hybridization prediction. *Nucleic Acids Res* **31**, 3406–3415.

Supplementary material

The following supplementary material is available online:

Doc. S1. Supplementary results and discussion.

Fig. S1. Effects of the pH of the binding buffer on reactions incubated at 0 °C and of temperature on reactions at pH 7.5 on binding of BcBL2 to PyrR as determined by filter binding.

Fig. S2. Sedimentation velocity studies on native and His-tagged PyrR at moderate ionic strength.

Fig. S3. An approach to equilibrium study with the native PyrR at low ionic strength.

Fig. S4. Equilibrium sedimentation studies of native and His-tagged PyrR at low ionic strength and concentrations shown.

Table S1. Structural variants of purine and pyrimidine nucleotides that affect binding of PyrR to BcBL2 as determined by filter binding.

Table S2. Apparent RNA dissociation constants (K_d values) for binding of structural variants of BcBL2 to PyrR.

Table S3. Sedimentation velocity analysis of native and His-tagged PyrR.
Table S4. Sedimentation velocity constants from the titration of BcBL2 with PyrR.

This material is available as part of the online article from http://www.blackwell-synergy.com

Please note: Blackwell Publishing are not responsible for the content or functionality of any supplementary materials supplied by the authors. Any queries (other than missing material) should be directed to the corresponding author for the article.